Food Chemistry: X 25 (2025) 102152

Contents lists available at ScienceDirect

Food Chemistry: X

journal homepage: www.sciencedirect.com/journal/food-chemistry-x

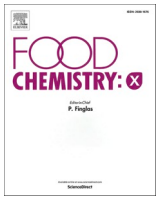

Vertical flow immunoassay for multiplex mycotoxins based on photonic nitrocellulose and SERS nanotags

Ruipeng Chen [a], Jingfang Hu [d], Hui Wang [a], Cheng Li [e], Haiqi Kang [f], Yuxuan Chen [a], Liang Yang [a], Xiangfang Tang [a,*], Benhai Xiong [a,*], Xiangwei Zhao [b,c,**]

[a] State Key Laboratory of Animal Nutrition and Feeding, Institute of Animal Science, Chinese Academy of Agricultural Sciences, Beijing 100193, PR China
[b] State Key Laboratory of Digital Medical Engineering, School of Biological Science and Medical Engineering, Southeast University, Nanjing 210096, China
[c] Southeast University Shenzhen Research Institute, Shenzhen 518000, China
[d] Beijing key Laboratory of Sensor, Beijing Information Science & Technology University, Beijing 100101, China
[e] Institute of Food Science and Technology, Chinese Academy of Agricultural Sciences, Beijing 100193, PR China
[f] College of Economics and Management, Beijing University of Agriculture, Beijing 102206, China

ARTICLE INFO

Keywords:
Surface-enhanced Raman scattering
Vertical flow assay
Photonic nitrocellulose (PNC)
Slow-photon effect
Multiplex mycotoxin detection

ABSTRACT

Here, we report a SERS based VFA using PNC as a sensing substrate for highly sensitive multiplex mycotoxins detection. The PNC was fabricated by filtration-based self-assembled monodisperse SiO_2 NPs on a filter membrane as a template, and the obtained PNC had an ordered complementary inverse opal structure. In parallel, three kinds of Raman dyes encoding Au@^{NBA}Ag, Au@$^{4\text{-}MBA}$Ag and Au@^{DNTB}Ag SERS nanotags were synthesized for the detection of OTA, AFB1 and ZON. In the immunoassay, because of the slow-photon effect of the PNC substrate, which facilitates the light coupling with SERS nanotags, the SERS signal was highly enhanced. The LODs of 8.2, 13.7 and 47.6 fg mL^{-1} were achieved for simultaneous detection of OTA, AFB1 and ZON, respectively, which were lower than the tolerable cutoff values recommended by the EC. Therefore, this proposed PNC based SERS VFA is expected to be a powerful method for multiplex mycotoxins detection.

1. Introduction

Contamination of agricultural products by mycotoxins is a serious problem worldwide because of their biological persistence and high toxicity. Ochratoxin A (OTA), aflatoxin B1 (AFBl), and zearalenone (ZON) are the most important mycotoxins, produced by secondary metabolites of several fungal species (Zinedine et al., 2007). Owing to improper storage or unusual weather conditions, contamination caused by AFBl, OTA, and ZON frequently occurs in cereal products and agricultural commodities such as wheat, corn, soybean, and rice. Moreover, these mycotoxins are potent toxins, and the consumption of contaminated products can have many adverse effects on humans and animals, such as teratogenesis, carcinogenicity, nephrotoxicity, immunosuppression, neurotoxicity, mutagenicity, and oestrogen effects (Kearns et al., 2017; Song et al., 2021). Owing to the high toxicity of mycotoxins to human health, many countries have set stringent limits for mycotoxin residues in food and feedstuffs. For example, the European Commission (EC) has established maximum permitted AFB1, OTA and ZON levels of 2, 5 and 100 μg kg^{-1}, respectively, in cereals (EC, 2006). For the effective control of mycotoxins and guarantee of consumer health, accurate and quantitative detection approaches with high sensitivity in food safety and animal husbandry are particularly imperative (Aichinger et al., 2020; Guo et al., 2019). At present, the commonly used mycotoxin detection methods include electrochemical aptamer sensors (Jalalian et al., 2018), fluorescent sensors (Regiart et al., 2018), high -performance liquid chromatography (HPLC) (Lin et al., 2018), liquid chromatography-mass spectrometry (LC-MS) (Santis et al., 2017), and enzyme-linked immunosorbent assay (ELISA) (Lai et al., 2017). Although HPLC and LC-MS can yield accurate test results, they need to be carried out in a well-equipped laboratory with well-trained professionals. However, electrochemical aptamer sensors, fluorescent sensors, and ELISA-based methods still have the disadvantage of low sensitivity. In addition, these methods require a long sample pretreatment time and the cost is high. Therefore, the development of

* Corresponding authors.
** Corresponding author at: State Key Laboratory of Digital Medical Engineering, School of Biological Science and Medical Engineering, Southeast University, Nanjing 210096, China.
E-mail addresses: tangxiangfang@caas.cn (X. Tang), xiongbenhai@caas.cn (B. Xiong), xwzhao@seu.edu.cn (X. Zhao).

https://doi.org/10.1016/j.fochx.2024.102152
Received 5 December 2024; Received in revised form 10 December 2024; Accepted 30 December 2024
Available online 31 December 2024

convenient, low-cost, and high-precision assay methods for multiplex mycotoxin detection is urgently needed.

The vertical flow immunoassay (VFA) using surface-enhanced Raman scattering (SERS) nanoprobes as a substitute for gold NPs has been proven to be a highly sensitive point-of-care testing (POCT) detection technology. This method has the advantages of not only fast analysis, simple operation, and no hook effect but also high sensitivity, multiplex coding capability and stability. In recent years, SERS VFA technology has been widely used for the detection of different biological targets or chemical analyses (Berger et al., 2017; Chen et al., 2019; Clarke et al., 2017; Zhang et al., 2019). Nevertheless, the current substrates used in SERS VFA detection are mainly porous nitrocellulose (NC) or cellulose acetate (CA) membranes, which have the disadvantages of inconsistent pore sizes and microstructures. For this reason, the distributions of gold nanoparticles or SERS nanotags on these substrates are uneven, which greatly reduces the repeatability and accuracy of the test signal. In addition, these substrates also suffer from high fluorescence background signal, which will further reduce the sensitivity of the detection signal.

Currently, materials with photonic crystal (PC) structures provide a new strategy to solve these problems. By using self-assembly technology, an ordered porous photonic nitrocellulose (PNC) with a periodic structure was prepared and used as the detection substrate for SERS VFAs. The PNC substrate with a reverse opal structure could further enhance the local electromagnetic field through the slow light effect, which is conducive to improving the detection signal of the SERS nanotag (Chen et al., 2008; Mu et al., 2015). In addition, compared with the traditional disordered substrate, the ordered porous structure detection substrate has the following advantages: First, the highly ordered nanoscale structure exhibits nonconfinement effect, which is conducive to mixing the detection reagents and improving the immunoassay efficiency. Second, by changing the size of the self-assembled silica particles, the pore size of the detection substrate can be easily changed to improve the coupling efficiency of excitation light with the SERS nanotag. Since self-assembled silica particles are used as templates for making ordered porous PNC membranes, the pore size of the prepared substrates can be controlled. The results show that the linear dynamic range of detection can be widened and that the detection sensitivity can be improved by choosing a PNC membrane with an appropriate pore size. In view of the above advantages of the ordered PNC detection substrate, its integration into the SERS VFA biosensor can further enhance its advantages in POCT applications.

In this study, as a proof of concept, a SERS VFA platform employing an ordered porous PNC membrane as the detection substrate and hypersensitive SERS nanotags for simultaneous detection of the three kinds of mycotoxins was constructed. Accordingly, the core-shell SERS nanotags with bimetallic structures, namely, Au^{NBA}@Ag, $Au^{4\text{-}MBA}$@Ag and Au^{DNTB}@Ag were fabricated and used as labels for OTA, AFB1 and ZON, respectively. A competitive SERS immunoassay was carried out between free mycotoxin targets and mycotoxins conjugated with bovine serum albumin (BSA) fixed on the PNC membrane, which competitively bind with mycotoxin antibody-conjugated SERS nanoprobes. Moreover, the structure of the ordered PNC and its preparation process are shown in Fig. 1a. Fig. 1b shows a schematic diagram of SERS VFAs based on an ordered PNC membrane for multiplex mycotoxin detection. Because the slow light effect of the ordered PNC membrane facilitated the coupling of excited light with the SERS nanoprobes, high sensitivity for mycotoxin detection could be achieved. Therefore, the detection platform is expected to be used for rapid detection and analysis of toxin factors in the field.

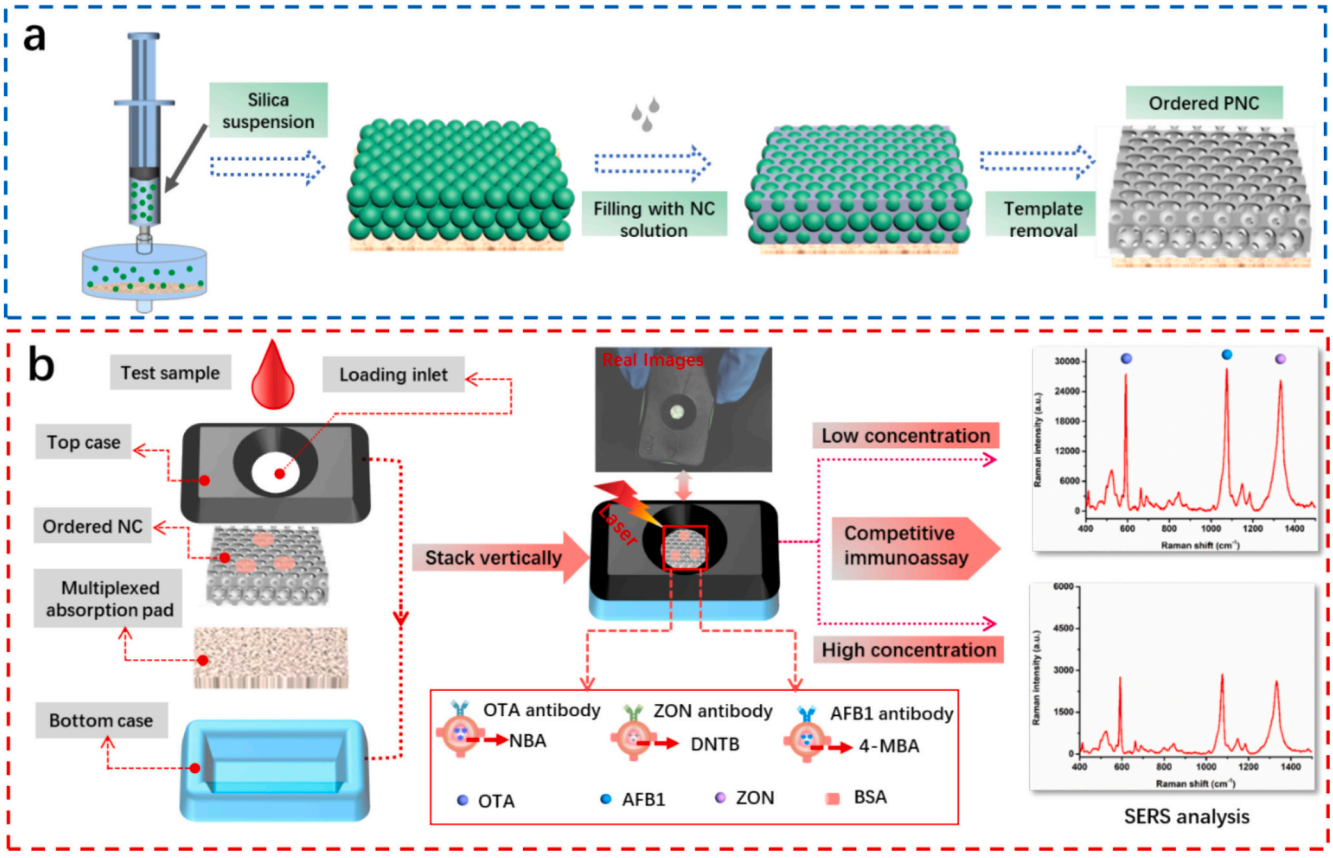

Fig. 1. SERS VFA biosensor based on an ordered PNC membrane and SERS nanotags for multiplex mycotoxin detection. (a) Synthesis of an ordered PNC membrane with SiO_2 particles and (b) schematic of multiplex mycotoxin (OTA, AFB1 and ZON) detection with the proposed biosensor.

2. Materials and methods

2.1. Chemicals, materials, and apparatus

Trisodium citrate ($Na_3C_6H_5O_7$), hydrogen tetrachloroaurate (III) trihydrate ($HAuCl_4{\cdot}3H_2O$), silver nitrate ($AgNO_3$), and hydrofluoric acid were purchased from Sigma-Aldrich (St. Louis, MO, USA). Trichloromethane and dimethyl sulfoxide were purchased from Alfa Aesar Co.. L-Ascorbic acid (AA), potassium carbonate (K_2CO_3), bovine serum albumin (BSA), hydrochloric acid (HCl), phosphate buffered saline (PBS, 0.01 M, pH = 7.4), phosphate buffered saline Tween-20 (PBST) and acetone were obtained from National Pharmaceutical Group Corporation (Beijing, China). For the preparation of the SERS nanotag, Raman molecule 4-mercaptobenzoic acid (4-MBA) was obtained from Sinopharm Chemical Reagent Co. (Shanghai, China). 5, 5′-Dithiobis (2-nitrobenzoic acid) (DNTB) was obtained from J&K Scientific Ltd.. Nile blue A (NBA) was obtained from Bodi Chemical Reagents Co. (Tianjin, China). Chemical standards of OTA, AFB1, ZON, anti-OTA monoclonal antibody (mAb), anti-AFB1 mAb and anti-ZON mAb, as well as OTA-BSA, AFB1-BSA and ZON-BSA conjugates, were obtained from Binzhou Honglan Biotechnology Co., Ltd. (Shandong, China). Nitrocellulose was purchased from Sinopharm Chemical Reagent Co., Ltd. (Shanghai, China). The monodisperse SiO_2 nanoparticles of different diameters were obtained from Nanjing Caina Biotechnology Co., Ltd. OTA, AFB1 and ZON enzyme-linked immunosorbent assay (ELISA) kits were purchased from Huaan Magnech Bio-Tech Co., Ltd. (Beijing, China). The filter holder, Whatman filter paper, and nylon filter membranes (0.22 μm, 25 mm in diameter) were purchased from Wanqing (Nanjing, China). Milli-Q water (resistivity of 18.0 MΩ cm, Millipore) was used to prepare all the chemical solutions.

2.2. Instrument

Scanning electron microscopy (SEM; Zeiss, Ultra Plus) with an accelerating voltage of 200 kV was used to characterize the AuNPs and PNC membranes. The structure of the core-shell SERS nanotag was analyzed by transmission electron microscopy (TEM; JEOL, JEM-2100) with an acceleration voltage of 200 kV. The TEM samples were prepared by dropping 3 μL of the NP suspension onto a copper grid coated with a carbon film and then evaporating it with a heating bulb. UV–Vis absorption spectra of the colloidal NPs were measured in a disposable polystyrene cuvette via a Mapada UV-6100 spectrometer with scanning wavelengths ranging from 300 to 800 nm. The reflection spectra were acquired by an optical fiber spectrometer (Ocean Optics, QE65000). Moreover, all SERS spectra were determined via a confocal Raman microscope system (Renishaw, UK). Most of the SERS spectra were acquired via a 785 nm laser at a power of 10 mW with an integration time of 10 s. In addition, SERS spectra were obtained from 300 to 1800 cm^{-1} with baseline correction to prevent background fluorescence. The antibody- conjugated Au^{NBA}@Ag, $Au^{4\text{-}MBA}$@Ag and Au^{DNTB}@Ag SERS nanoprobes were used to detect OTA, AFB1 and ZON, respectively. The quantitative analysis of the spectra was performed with OriginPro 2016.

2.3. Preparation of the gold core silver shell SERS nanotags

Gold core silver shell SERS nanotags were synthesized via a commonly used protocol with some adjustments (Chen et al., 2020). Accordingly, AuNPs with a particle size of ~60 nm were fabricated according to the methods of Frens, and the details are described in Supporting Information S1 (Frens, 1973). For the preparation of the gold core silver shell SERS nanotags Au^{NBA}@Ag, $Au^{4\text{-}MBA}$@Ag and Au^{DNTB}@Ag, the Raman molecules NBA (5.0 μM, 1.0 mL), 4-MBA (10 μM, 0.5 mL) and DNTB (10 μM, 0.5 mL) were added dropwise to the colloidal gold solution, and the mixtures were stirred at 400 rpm for 30 min. Then, the Raman molecules attached AuNPs (Au^{NBA}, $Au^{4\text{-}MBA}$ and Au^{DNTB}) were centrifuged twice at 4000 rpm for 10 min, and the sediments were resuspended in deionized water. After that, 1 mL of 0.01 M AA and 0.5 mL of 0.025 M $AgNO_3$ were successively added to Raman dyes attached Au^{NBA}, $Au^{4\text{-}MBA}$ and Au^{DNTB}, respectively. Owing to the reduction of $AgNO_3$ by AA, the solution gradually turned light yellow, demonstrating the successful coating of the Ag shell around the gold surface. After centrifugation, the synthesized core-shell SERS nanotags Au^{NBA}@Ag, $Au^{4\text{-}MBA}$@Ag and Au^{DNTB}@Ag were dispersed in the same volume of deionized water and stored at 4 °C in a refrigerator.

2.4. Preparation of the antibody-conjugated SERS nanotags

For the simultaneous detection of the multiplex mycotoxins OTA, AFB1 and ZON on one test spot, each antigen should be recognized by its characteristic spectral signatures from various distinct SERS nanotags. Accordingly, the pH values of the three kinds of SERS nanotags (Au^{NBA}@Ag, $Au^{4\text{-}MBA}$@Ag, and Au@^{DNTB}Ag) were adjusted to 8.5 with HCl and K_2CO_3 solutions, mixed with labelled anti-OTA, anti-AFB1 and anti-ZON, respectively, and incubated in an incubator at 37 °C for one hour. Afterwards, the anti-OTA-conjugated Au^{NBA}@Ag NPs, anti-AFB1-conjugated $Au^{4\text{-}MBA}$@Ag NPs and anti-ZON-conjugated Au@^{DNTB}Ag NPs were mixed with 2 mL of 3 % BSA to block any unreacted sites on the Ag shell surface of the Au@Ag SERS nanotags. After that, the mixture was centrifuged at 6000 rpm for 20 min to remove the excess reagent. Thereafter, the antibody-conjugated SERS nanotags were resuspended in PBS solution supplemented with BSA (0.2 %, *w*/w), and stored at 4 °C until use.

2.5. Fabrication of the ordered porous PNC membrane

Fig. 1a shows an ordered porous PNC membrane with an inverse-opal structure fabricated by a previously reported method with some modifications (Gao et al., 2016). First, monodisperse SiO_2 nanoparticles (35 %, w/w) were filtered vertically through a nylon membrane via a syringe. After drying for 2 h (30 °C, relative humidity of 50 %), a template with an ordered hexagonal close-packed structure was formed on the nylon membrane. The NC solution prepared with acetone and dimethyl sulfoxide (1:1, *v*/v) was subsequently deposited dropwise onto the template and infiltrated into the nanopores of the self-assembled crystal template via capillary force. Afterwards, it was solidified in an oven at 60 °C for 3 h and immersed in a 4 % hydrofluoric acid solution for 4 h to etch the silica nanoparticles. Finally, an ordered PNC membrane with a structure complementary to that of the self-assembled silica PC template was obtained and used as a sensing substrate in the SERS VFA biosensor.

2.6. Immobilization of biomarkers on the PNC membrane

For the immobilization of antigens on the sensing substrate, the ordered PNC membrane was first treated in an oxygen plasma cleaner (10 min, 80 W) to modify the hydroxyl groups on its surface. Then, the sample were immersed in a PBS solution containing 0.05 % Tween-20 for one hour and washed three times with deionized water. Thereafter, mixtures of OTA-BSA, AFB1-BSA, and ZON-BSA (1 mg mL^{-1}, volume ratio of 1:1:1) were deposited on the substrate dropwise to generate three round detection regions.

2.7. Detection of multiplex mycotoxins

To detect the three mycotoxins OTA, AFB1 and ZON simultaneously, a competitive immune reaction was employed in this PNC membrane-based SERS VFA platform. First, uniformly mixed antigens of OTA-BSA, AFB1-BSA and ZON-BSA (1 mg mL^{-1}, volume ratio of 1:1:1) were fixed in the three detection regions of the ordered PNC membrane-based SERS VFA biosensor. Then, the prepared anti-OTA mAb labelled Au^{NBA}@Ag, anti-AFB1 mAb labelled $Au^{4\text{-}MBA}$@Ag, and anti-ZON mAb labelled Au^{DNTB}@Ag were mixed with different concentrations (1 μg

mL^{-1}-10 fg mL^{-1}) of the toxin standards OTA, AFB1 and ZON. After several minutes, they were deposited onto the detection area for a competitive reaction. Under suitable conditions, the binding ability of toxins and antibodies was greater than that of artificial antigens (OTA-BSA, AFB1-BSA and ZON-BSA) and antibodies. Therefore, with increasing toxin concentration, the intensity of the characteristic peaks of the mixed SERS spectra in the detection area gradually decreased, laying a foundation for establishing the relationship between the spectral intensity and toxin concentration. Notably, each concentration gradient was measured in triplicate.

2.8. Natural food sample preparation

The fresh corn, wheat samples were purchased from a local market, and certified as free of OTA, AFB1 and ZON. Then, the obtained cereals were ground by a high-speed disintegrator, until it became thin power. Next, two grams of each sample and 10 mL methanol-water (70:30, *v*/v) were added to 15 mL centrifuge tubes, and vortexed vigorously for 5 min. After 30 min shaking, the extraction of the samples were carried out by 15 min centrifugation at 5000 rpm at 25 °C. The supernatant was transferred to a 2 mL tube, and used as blank sample. Subsequently, the various concentrations of AFB1, OTA and ZON standard solutions were spiked into blank sample and completely mixed by vortex, respectively. Thereafter, those mixtures were put into the oven at 37 °C overnight for the solvent to completely evaporate. The spiked samples were extracted with 3 mL of trichloromethane and filtered with Whatman filter paper. After the collected filtrates dried in an oven at 65 °C, the extracted samples were dissolved into 2 mL of PBS buffer. The control samples were extracted in the same conditions. Eventually, the samples were measured by the proposed method, and the validation assays using ELISA kits were performed according to ELISA instructions.

3. Results and discussion

3.1. Optimization and characterization of the SERS nanotags

For the quantitative analyses of multiple mycotoxins OTA, AFB1 and ZON, Raman molecules (NBA, 4-MBA and DNTB) encoding gold core silver shell SERS nanotags were prepared as nanoprobes. The nanoprobes were fabricated by a frequently used seed-mediated growth method, and their structure is schematically illustrated in Fig. 1b. It has been reported that gold nanoparticles (NPs) ~ 60 nm in size have better SERS effects than others (Krug et al., 1999); therefore, we chose to synthesize ~60 nm gold NPs. Fig. S1a (Supporting Information) shows a TEM image of the prepared gold NPs with a diameter of 58.6 ± 4.32 nm. Fig. S1b (Supporting Information) also shows that the size distribution of the gold NPs was very fine, which was necessary for the preparation of the Au@Ag SERS nanotags. Nevertheless, the intensity and stability of the prepared SERS nanotags are critical for quantitative analysis. Therefore, optimizing the ultrasensitivity and reproducibility of the synthetic SERS nanotags is essential. Taking the $Au^{4\text{-MBA}}$@Ag nanoparticles (NPs) as an example, 4-MBA molecules were attached to the surface of the Au NPs via disulfide linkages and subsequently surrounded by a Ag layer. The SERS signal of $Au^{4\text{-MBA}}$@Ag depended strongly on the electromagnetic enhancement originating from the localized surface plasmon resonance (LSPR) within the interstice of Au@Ag NPs, which was greatly affected by the thickness of the Ag shell (Liu et al., 2019). Therefore, different amounts of $AgNO_3$ with concentrations of 0.025, 0.05, 0.075, 0.1, 0.125, and 0.15 mM were optimized to ensure the highest Raman intensity at 1076 cm^{-1}. As the amount of $AgNO_3$ increased, the colour of the solution slowly transitioned from a purplish-red to orange yellow (Fig. 2a). In addition, with increasing $AgNO_3$ concentration, the SPR of the Ag absorption peak (approximately 400 nm) increased, whereas the Au absorption peak blue-shifted, indicating increase in the thickness of the Ag shell encapsulated on the gold NPs (Fig. 2b). The SERS intensity of $Au^{4\text{-MBA}}$@Ag with different amounts of $AgNO_3$ at 1076 cm^{-1} is shown in Fig. 2c. $Au^{4\text{-MBA}}$@Ag exhibited a higher SERS intensity than did $Au^{4\text{-MBA}}$. Furthermore, with increasing amounts of $AgNO_3$, the SERS intensity steadily increased and reached a maximum value at 0.1 mM $AgNO_3$. This may be due to the increase in the thickness of the Ag shell, which strengthened the confined electromagnetic field of the intergap of the core-shell SERS nanotag and improved the SERS intensity (Liu et al., 2017). However, when the amount of $AgNO_3$ was greater than 0.1 mM, the Raman intensity of $Au^{4\text{-}}$

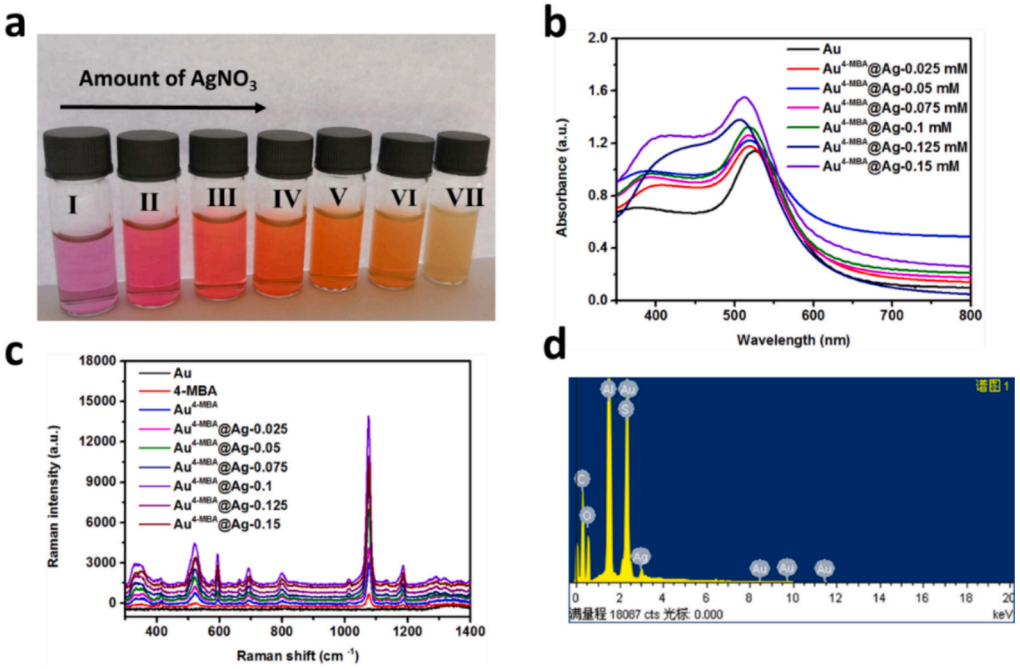

Fig. 2. (a) digital photographs of 0 (I), 0.025 (II), 0.05 (III), 0.075 (IV), 0.1 (V), 0.125 (VI) and 0.15 (VII) mM $AgNO_3$ and (b) UV–Vis of Au NPs and the $Au^{4\text{-MBA}}$@Ag NPs, and (c) Raman intensity of 4-MBA at 1076 cm^{-1} of $Au^{4\text{-MBA}}$@Ag NPs with different amount of $AgNO_3$. (d) The element mapping image of EDS on $Au^{4\text{-MBA}}$@Ag NPs.

^{MBA}@Ag began to decrease, which was attributed to the thicker Ag layer shielding the SERS signal, resulting in a weaker SERS intensity. Thus, 0.1 mM $AgNO_3$ was chosen as the optimum volume for preparing the SERS nanotags.

Furthermore, based on the above optimal conditions, a TEM image of the Au$^{4\text{-MBA}}$@Ag core-shell SERS nanotag is displayed in Fig. 3a. The SERS nanotags had good uniformity and dispersity and had a size distribution of approximately 63 ± 3.56 nm (Fig. 3b). Moreover, the edge of the SERS nanotags was much brighter than the center core, and X-ray energy dispersive spectroscopy (EDS) analysis revealed the existence of Au, S, and Ag elements in the nanoparticles (Fig. 2d), both of which demonstrated that the Au$^{4\text{-MBA}}$@Ag core-shell SERS nanotags were prepared. To further confirm the structure of Au$^{4\text{-MBA}}$@Ag, STEM characterization and elemental mapping of silver, gold, and sulfur were also conducted via high-resolution transmission electron microscopy (HRTEM). As shown in Fig. 3c, a thin grayish silver layer encircled the bright gold core. In addition, Au, S, and Ag elements are indicated by yellow, green, and red colors, respectively. The merged image indicates a distinct core-shell structure and 4-MBA molecules were embedded between the gap of core-shell nanostructure. The resulting SERS nanotags must be conjugated with antibodies and can be used as labels in our biosensor.

Thus, UV–vis absorption spectra were obtained and are shown in Fig. 3d. The initial absorption peak of the ~60 nm gold NPs was 535 nm, and then blue shift to 525 nm after the formation of Ag shell. The absorption peak subsequently redshifted from 525 to 530 nm following the attachment of the antibodies, confirming the successful linkage of the antibodies. Moreover, the UV–vis absorption spectra of Au, Au$^{4\text{-MBA}}$@Ag, and Au$^{4\text{-MBA}}$@Ag-antibody are distinct and symmetric, demonstrating that they also have good dispersibility. Furthermore, the zeta potential values of Au, Au$^{4\text{-MBA}}$, Au$^{4\text{-MBA}}$@Ag and Au$^{4\text{-MBA}}$@Ag-Ab are −38 ± 3.8, −33 ± 2.5, −36 ± 3.3, and − 25 ± 2.7, respectively, the change of the zeta potential values shown in Fig. S2 (Supporting Information) also indicates the successful modification of these nanoparticles. All these results demonstrated that our synthesized gold core silver shell SERS nanotags have great potential to serve as signal reporters in our next application.

3.2. SERS spectra analysis

For this newly established PNC membrane integrated SERS immunoassay, Raman molecules modified Au core Ag shell SERS nanoprobes were selected as the coding elements for the precise and extensive detection of various mycotoxins. Therefore, the encoding ability and SERS intensity of SERS nanotags are important issues to consider. In accordance with the previous studies (Chen et al., 2020), NBA, 4-MBA and DNTB were chosen to encode the Au^{NBA}@Ag, Au$^{4\text{-MBA}}$@Ag, and Au^{DNTB}@Ag SERS nanotags for the detection of OTA, AFB1 and ZON, respectively. The Raman spectra of these three SERS nanotags are displayed in Fig. 4. The Raman peaks at 593, 1076 and 1335 cm^{-1} are attributed to Au^{NBA}@Ag, Au$^{4\text{-MBA}}$@Ag, and Au^{DNTB}@Ag, respectively. Generally, the Raman shift of NBA at 593 cm^{-1} was assigned to the ν_s (C_3-O_{20}-C_8) or ν_s (C_4-N_{19}-C_7) ring-II breathing mode (Mažeikienė et al., 2019). The Raman peak of 4-MBA at 1076 cm^{-1} was attributed to the coupling of the in-plane ring vibrational mode with the ν(C—S) vibration mode (Zhou et al., 2018). Furthermore, DNTB had a dominant Raman band at 1335 cm^{-1}, which was attributed to the symmetric nitro stretching vibration (Gellner et al., 2009). Notably, even though the

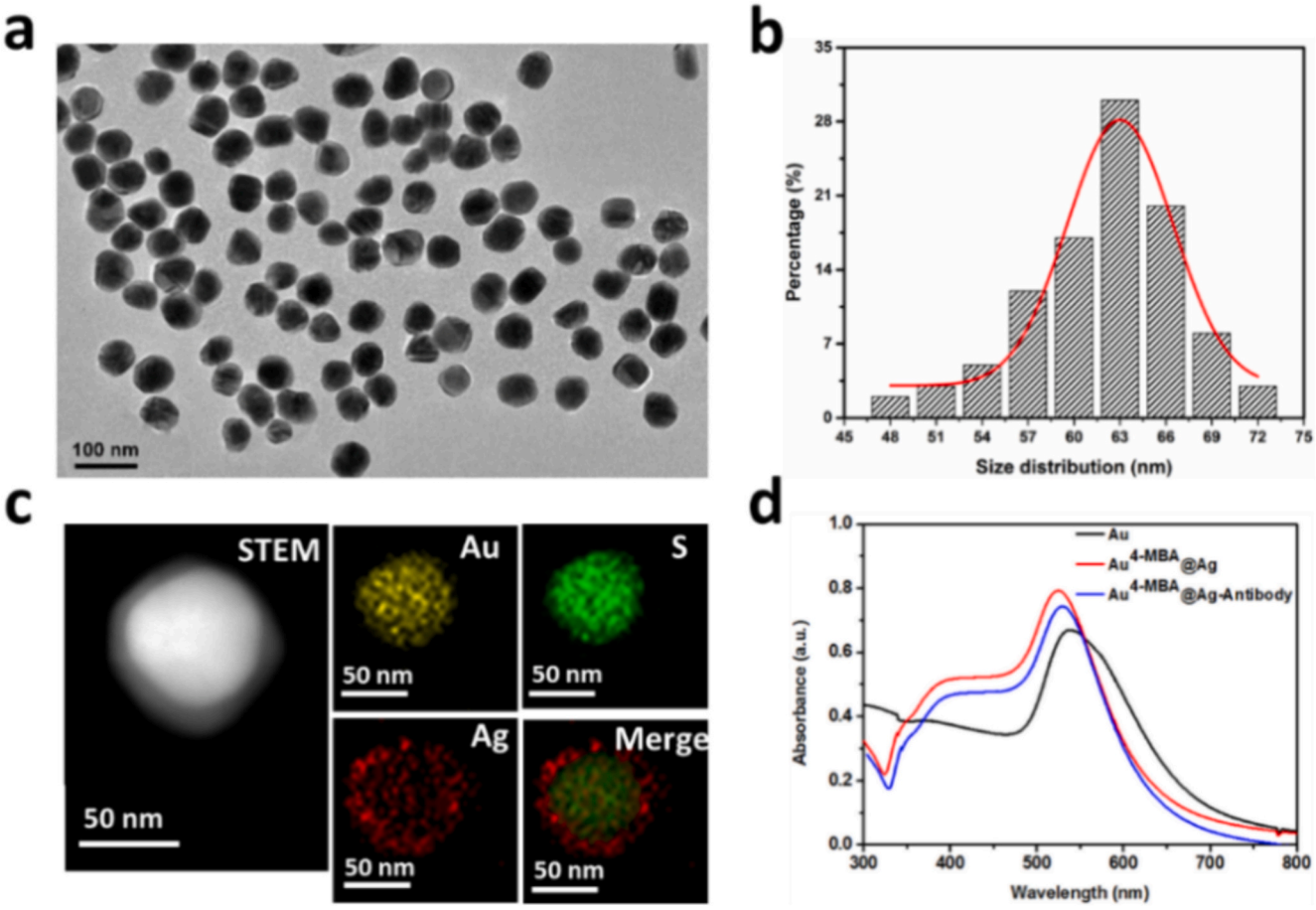

Fig. 3. (a) TEM image and (b) size measurement of the Au$^{4\text{-MBA}}$@Ag SERS nanotags. (c) STEM image and elemental mapping of the Au$^{4\text{-MBA}}$@Ag core-shell SERS nanotag via HRTEM. (d) UV–vis spectra of AuNPs, Au$^{4\text{-MBA}}$@Ag SERS nanotags and antibodies bio-conjugated Au$^{4\text{-MBA}}$@Ag SERS nanotags.

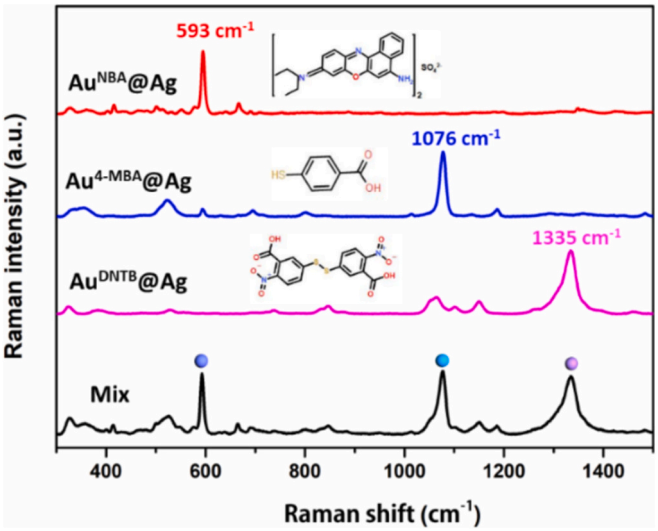

Fig. 4. Raman spectra of Au^{NBA}@Ag (first line), $Au^{4\text{-}MBA}$@Ag (second line), and Au^{DNTB}@Ag (third line) and their equimolar mixtures (fourth line). The Raman shifts at 593, 1076 and 1335 cm^{-1} were used for the quantitative detection of OTA, AFB1 and ZON, respectively.

Raman shifts at 593 cm^{-1} for Au^{NBA}@Ag and 588 cm^{-1} for $Au^{4\text{-}MBA}$@Ag and at 1076 cm^{-1} for $Au^{4\text{-}MBA}$@Ag and 1063 cm^{-1} for Au^{DNTB}@Ag were very close, there was no overlap between them, which can be further confirmed in Fig. S3 (Supporting Information). Moreover, the intensities of the three characteristic Raman peaks were essentially similar, indicating that the Au^{NBA}@Ag, $Au^{4\text{-}MBA}$@Ag and Au^{DNTB}@Ag selected were suitable for multiplex mycotoxin detection without further deconvolution. Furthermore, as shown in Fig. S4 (Supporting Information), it can be seen that the intensities after antibodies grafting lightly decreased and remained on the same order of magnitude for the three kinds of SERS nanotags. Therefore, Au^{NBA}@Ag, $Au^{4\text{-}MBA}$@Ag and Au^{DNTB}@Ag can be served as labels in this PNC membrane integrated SERS VFA for the highly sensitive detection of OTA, AFB1 and ZON, respectively.

3.3. Optimization of the concentration of the NC solution

The methodology used to fabricate the ordered porous PNC membrane with good uniformity is outlined in Fig. 1a. First, 300 nm monodisperse silica microspheres were vertically infiltrated on the nylon substrate to fabricate a self-assembled ordered template. The cross-sectional SEM image shown in Fig. S5 (Supporting Information) reveals that the SiO_2 template was densely and uniformly packed layer by layer without obvious aggregation and clustering. Then, the nitrocellulose (NC) solution was added to the template. In this procedure, propelled by capillary forces, the NC solution seeped into the interstices of the SiO_2 PC template and supplanted the air that trapped among the SiO_2 NPs. Finally, an ordered PNC membrane was obtained after removing the SiO_2 PC template. Notably, the concentration of NC solution had a direct effect on the formation of the PNC membrane. Thus, the optimization of different concentrations of NC solution was investigated. As shown by the SEM images in Fig. 5, six different concentrations of NC solution were added to the ordered template. Fig. 5 (a) shows that when the concentration of the NC solution was 12 %, the formed NC film was too thick and covered the ordered template, which was not conducive for hydrofluoric acid etching of SiO_2 NPs to form an ordered porous PNC membrane. The concentrations of the NC solutions were subsequently decreased to 9 % and 6 %, and their SEM images are displayed in Fig. 5b and c, respectively. Although the ordered self-assembled SiO_2 template could be observed, slight defects and cracks appeared, which may affect the integrity of the formed PNC membrane. The reasons for this finding may be that, due to the high concentration and viscosity of the NC solution, it was easy to shift the ordered template during the diffusion process, which was not beneficial for the formation of an ordered PNC membrane. Next, the concentration of the NC solution was changed to 4 %, as shown in Fig. 5d, the ordered silica template could be clearly seen, and the diffusion of the NCs on the ordered template was more uniform, which was instrumental in the formation of an ordered porous PNC membrane with a uniform thickness. However, when the NC concentration continued to decrease to 2 % and 1 %, as shown in Fig. 5e and f, the NC membranes that formed after diffusion were not uniform or were essentially unable to form PNC membranes with ordered porous structures. Moreover, the mechanical strength of the obtained membranes was relatively weak, which was detrimental to the preparation of the ordered porous PNC membrane. Therefore, under

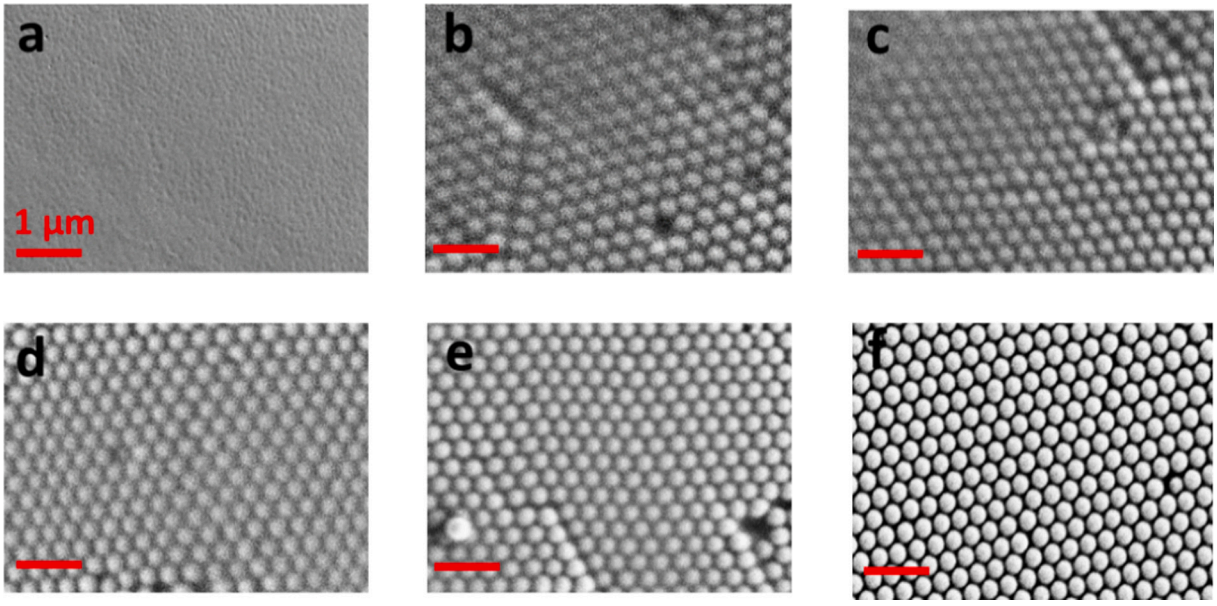

Fig. 5. SEM images of different concentrations of NC solution diffused on SiO_2 PC templates for the fabrication of ordered PNC template. The concentrations of NC solution for a, b, c, d, e, and f were 12 %, 9 %, 6 %, 4 %, 2 % and 1 %, respectively. Scale bar: 1 μm.

consideration of the optimization of NC solution concentration, the concentration of 4 % was selected to prepare the ordered porous detection substrate.

3.4. Preparation and selection of the ordered porous PNC substrate

To prepare PNC membranes with different pore sizes, five kinds of monodisperse silica particles were injected into the nylon membranes through syringes, as shown in Fig. 1a. After self-assembly at room temperature for about 1 h, ordered silica PC templates in a hexagonal close-packed arrangement were obtained (Fig. 6a, b, c, d and e). Then, freshly prepared NC solution (4 % by mass) was dropped on the ordered SiO_2 PC template, and some of the NC solution would diffuse and penetrate in the interspace of the ordered silica SiO_2 PC template. Afterwards, the substrates were placed in an oven at 60 °C for about 3 h. After the substrates were completely dried, they were etched for 4 h in hydrofluoric acid solution to remove the silicon dioxide particles, forming ordered porous PNC membranes with inverse opal structures (Fig. 6f, g, h, i and j). In contrast, a nitrocellulose membrane with no template and a random pore structure was also fabricated (Fig. 6 k). Compared with the ordered porous PNC membranes, the random-structured NC showed a broad reflection spectrum and no obvious reflection peak (Fig. 6 l). The reason for this finding was that the ordered PNC membranes with ordered hole-like structures had a periodic microstructure, with the photon forbidden band generated by the Bragg scattering effect, and could selectively reflect photons with specific wavelengths (Fig. 6 l) (Chi et al., 2017). According to the literature, this kind of ordered porous PNC membrane with an inverse opal structure has a slow light effect that can further amplify the intensity of the SERS signal (Curti et al., 2017; Huang et al., 2010; Yu et al., 2018). Under suitable conditions, when the excitation wavelength was near the photonic forbidden band, the photon group velocity decreased greatly, which could enhance the interaction between light and matter and promote the coupling efficiency between light and noble metals in the local range. As a result, the intensity of the local electromagnetic field was enhanced, and the SERS signal was further enhanced (Fan et al., 1997; Sun et al., 2016; Zelsmann et al., 2003). In this study, as described below, a 785 nm wavelength laser was selected as the excitation light source, which is consistent with previous studies (Radmark et al., 2020; Tuschel, 2016). To match the photonic band gap of the prepared PNC membrane with the selected excitation light, the reflection peaks of PNC membranes with different pore sizes were measured and are shown in Fig. 6 l. The relationship between the pore size of the PNC membrane and the photonic band gap can be described by the following equation according to Bragg's law

$$\lambda = 1.633D\cdot\sqrt{n_{void}^2\cdot f + n_{air}^2\cdot(1-f) - sin^2\ \theta\lambda}$$

where λ is the wavelength of the photonic stop band; *D* is the distance

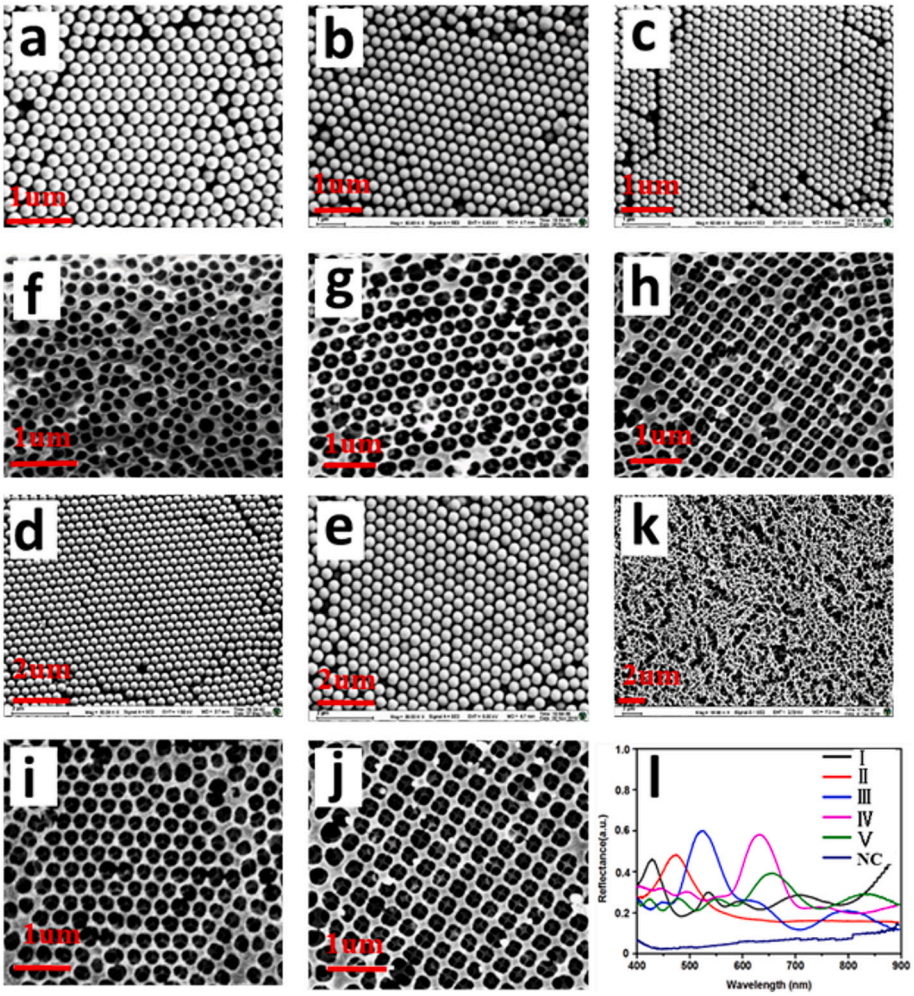

Fig. 6. (a-e) SEM images of the self-assembled SiO_2 templates used to manufacture ordered PNC membranes, (f-j) the corresponding as-prepared PNC membranes with different stopband wavelengths and (k) the irregularly structured NC membrane fabricated by directly depositing the NC solution onto the nylon membrane. The particle sizes of the SiO_2 NPs in a-e were 200, 230, 270, 300 and 430 nm, respectively. Scale bar: 1 μm. (l) Reflectance peaks of the fabricated substrates. The reflection peaks were at 428.6 nm (I), 472.2 nm (II), 523.1 nm (III), 632.4 nm (IV), and 652.2 nm (V), respectively.

between the centers of adjacent pores; n_{void} and n_{air} are the refractive indices of the voids (1.53 for NC) and air (1.0), respectively; f is the volume fraction of the host structure, which is taken as 0.26 for the inverted opal structures; and θ is the incident angle of the light in the normal incident direction, which is 0° in this study (Kuo et al., 2007; Sumioka et al., 2002; Zhao et al., 2009). The calculated photonic band gap of the 200 nm SiO_2 was approximately 380 nm, which was slightly smaller than the experimentally determined value of ~430 nm. This may be caused by inaccurate values of n_{void} and structural defects. Nevertheless, as the pore size increased, the reflection peak gradually redshifted, which was in accordance with Bragg's law, and gradually approached the wavelength of the excitation light. To evaluate the effect of the stopband wavelength on the SERS intensity, the same amount of Au^{NBA}@Ag (0.01 nM, 3.0 μL) was dropcast on each PNC substrate. Fig. S6 shows the SERS intensity of Au^{NBA}@Ag at 593 cm^{-1} or different PNC substrates. Obviously, the SERS intensity obtained for each of the PNC membrane was higher than that of the random-structured NC membrane. Furthermore, the PNC membranes (III, IV and V) with stopbands that were shifted slightly from λ_{ex} led to a significant increase in the SERS signal. Interestingly, although the band gap edges of IV and V were near 700 nm, the intensity of the reflection peak of IV (632.4 nm) was greater than that of V (652.2 nm). The SERS detection sensitivity is largely attributed to the enhanced matter-light interaction through repeated and multiple light scattering in the PNC membrane (Yu et al., 2018). Thus, the greatest enhancement was observed for the PNC membrane with a stopband of 632.4 nm, and it was employed for further SERS VFA experiments.

3.5. Comparison of the immunoassay results based on PNC and NC

In order to verify whether the performance of the PNC membrane-based SERS VFA was better than that of the commercially obtained traditional NC membrane, the biotoxin OTA (1 ng mL^{-1}) was detected via these two detection platforms. After washing, the SERS signals were measured with 532, 633 and 785 nm lasers, and the results are shown in Fig. 7a and b. The 785 nm laser exhibited better SERS performance than the 532 and 633 nm lasers did in both measurements. This occurred because the 785 nm laser not only reduced the background fluorescence signal of the Raman dye but also enhanced the electromagnetic field between the Au core and the Ag shell of the SERS nanotag, leading to improved SERS intensity. Furthermore, as shown in Fig. 7c, the SERS intensity and signal-to-noise ratio (SNR) of the ordered PNC membrane were greater than those of the random-structured NC membrane. The reason for this finding may be the slow light effect resulting from the laser being repeatedly scattered among the period voids, which increased the coupling efficiency between the excitation light and the SERS nanotags and improved the SERS signal. In addition, as shown in Fig. S7 (Supporting Information), more SERS nanotags were distributed on the ordered PNC membrane than on the random-structured NC. This occurred because the PNC membrane with periodic nanopores had nanoconfinement effect, which was favourable for immune reagent mixing and improving the binding kinetics of biomolecular reactions, resulting in the attachment of more immune complexes. To further prove this phenomenon, OTA at concentrations ranging from 100 pg mL^{-1}-1 μg mL^{-1} was tested by using an ordered PNC membrane and traditional NC as the sensing substrate for SERS VFAs. The average SERS

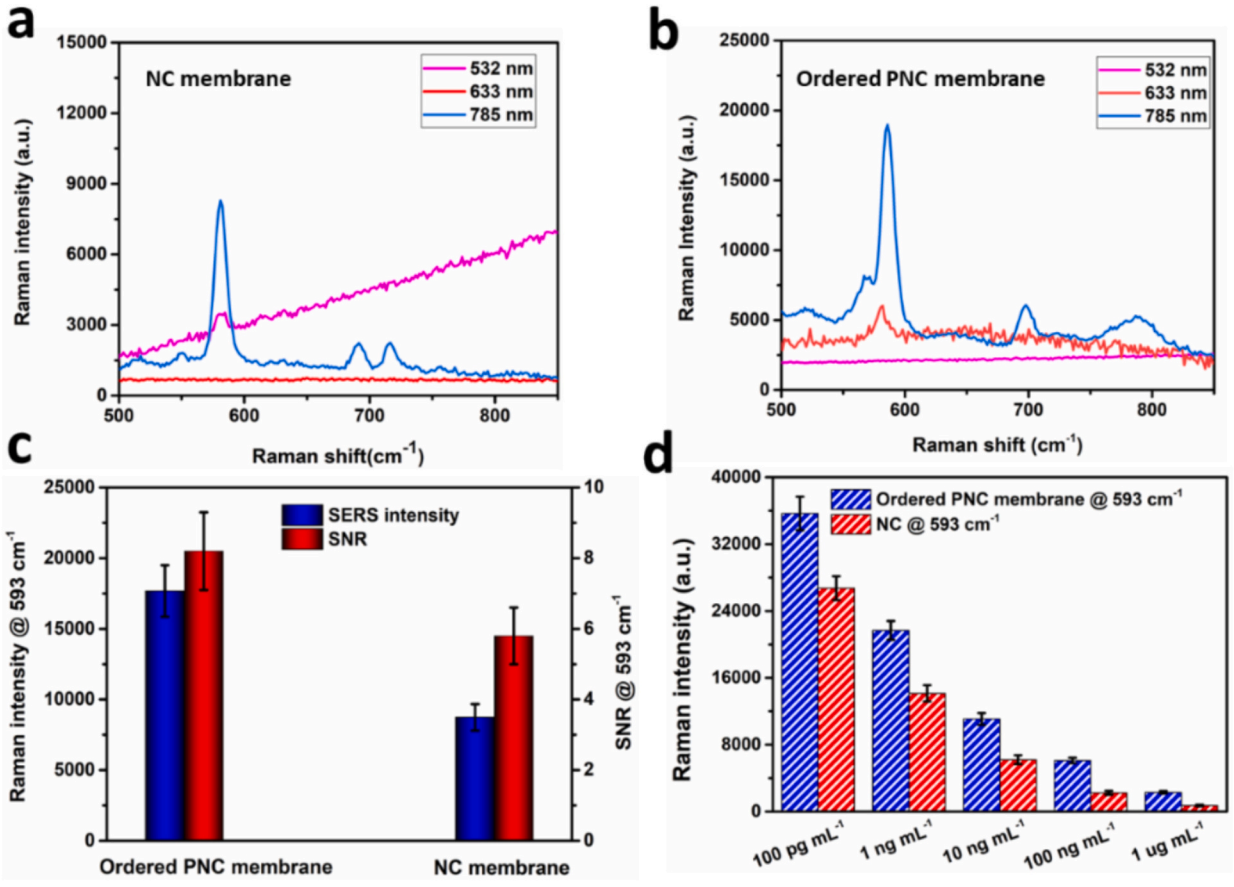

Fig. 7. Comparison of the performance of PNC that of NC in terms of SERS VFAs for the detection of OTA. (a, b) Raman spectra of the detection of 1 ng mL^{-1} OTA on the NC and ordered PNC membranes with three different laser wavelengths (532, 633 and 785 nm). (c) Effects of different sensing substrates (PNC vs. NC) on the Raman intensity and SNR at 593 cm^{-1} and (d) the Raman intensity at 593 cm^{-1} for the detection of various concentrations of OTA (0.1 ng mL^{-1}-1000 ng mL^{-1}) on the NC and ordered PNC membranes.

intensity with a Raman shift at 593 cm^{-1} for these samples at different concentrations is shown in Fig. 7d. With increasing concentrations of OTA, the SERS intensity of both biosensors decreased gradually. Moreover, the SERS intensity of the ordered PNC membrane was greater than that of traditional NCs. Therefore, the PNC membrane with an ordered inverse opal structure could facilitate light coupling with SERS nanotag by multiple light scattering and play a determinative role in improving the SERS detection sensitivity.

3.6. Evaluation of the performance of the PNC membrane-based SERS VFA

To evaluate the quantitative performance of this ordered PNC membrane-based SERS VFA for multiplex mycotoxin detection, the cross-reaction was verified since it is a key factor affecting the reliability and accuracy of the proposed immunoassay. For this purpose, mixtures of OTA-BSA, AFB1-BSA, and ZON-BSA capture antigens (0.1 mg mL^{-1}, volume ratio of 1:1:1) were immobilized on the test zone of the PNC membrane. Then, OTA of different concentrations (0.2–780 pg mL^{-1}) and AFB1 and ZON of fixed concentrations were added to the test zone after mixing with anti-OTA conjugated Au^{NBA}@Ag, anti-AFB1 conjugated $Au^{4\text{-}MBA}$@Ag and anti-ZON conjugated Au^{DNTB}@Ag (Table S1, Supporting Information). After immunoreaction, the SERS intensity was measured to determine the degree of cross-reaction. As shown in Fig. 8a and b, the SERS intensities of 4-MBA (1076 cm^{-1}) and DNTB (1335 cm^{-1}) remained constant, regardless of OTA concentrations. In comparison, the SERS intensity correlated with OTA decreased gradually with increasing of OTA concentration from 0.2 to 780 pg mL^{-1}, demonstrating that the cross-reaction was negligible. Similarly, in the other two test regions, AFB1 of different concentrations was blended with OTA and ZON at fixed concentrations, and ZON of different concentrations was blended with AFB1 and OTA at fixed concentrations. Analogous results were obtained, as shown in Figs. 8c, d, e and f, which indicated that no serious cross-reaction occurred among the analysts and that the proposed biosensor had good specificity and accuracy.

As a proof-of-concept, a potential application of the proposed SERS-based immunoassay for the quantitative multiplex detection of mycotoxins was conducted. First, equimolar mixtures of OTA-BSA, AFB1-BSA and ZON-BSA capture antigens were immobilized on the three test zones of the PNC sensing substrate. Multiplex detection of OTA, AFB1 and ZON at concentrations ranging from 10 fg mL^{-1}-1 μg mL^{-1} was subsequently performed using the corresponding SERS nanotags, namely, Au^{NBA}@Ag, $Au^{4\text{-}MBA}$@Ag, and Au^{DNTB}@Ag with Raman shifts at 593, 1076 and 1335 cm^{-1}, respectively. Finally, the measured average SERS intensities were used for quantitative analysis of mycotoxin content. As shown in Fig. 9a, the Raman intensity of the mixed SERS spectra at 593, 1076 and 1335 cm^{-1} became weaker gradually with increasing concentrations of OTA, AFB1 and ZON, and this trend was consistent with the competitive immune reaction. Accordingly, the quantitative relationships between the logarithmic concentrations of OTA, AFB1 and ZON and the corresponding SERS intensities at 593, 1076 and 1335 cm^{-1} were analyzed, and the results are shown in Figs. 9b, c and d, respectively. The three response curves were fitted with detection concentrations ranging from 10 fg mL^{-1} to 1 μg mL^{-1}. Furthermore, the inset figures show the linear section and R^2 values of the calibration curves. For OTA, as shown in the inset of Fig. 9b, the linear dynamic ranged (LDR) was from 10^{-3} to 10^{3} ng mL^{-1}, with an R^2 value of 0.978. As shown in the insets of Fig. 9c and d, the LDRs ranged from 10^{-3} to 10^{-2} ng mL^{-1}, with R^2 values of 0.938 and 0.969 for AFB1 and ZON, respectively. In addition, the limits of detection (LODs) were calculated from the average value of the blank sample plus 3 times the standard deviation of the blank sample signal (Nath & Ray, 2023). Consequently, the calculated LODs for OTA, AFB1 and ZON were 8.2, 13.7 and 47.6 fg mL^{-1}, respectively. These values all meet the European Commission (EC) recommended tolerable cut-off values (EC, 2006). Moreover, compared with that of other detection methods that use the same antibodies, the sensitivity of this proposed ordered PNC membrane-based SERS VFA biosensor for most mycotoxins was improved by at least two order of magnitudes (Table S2, Supporting Information).

3.7. Evaluation of the proposed biosensor for real sample detection

To evaluate the feasibility, reliability and accuracy of the PNC

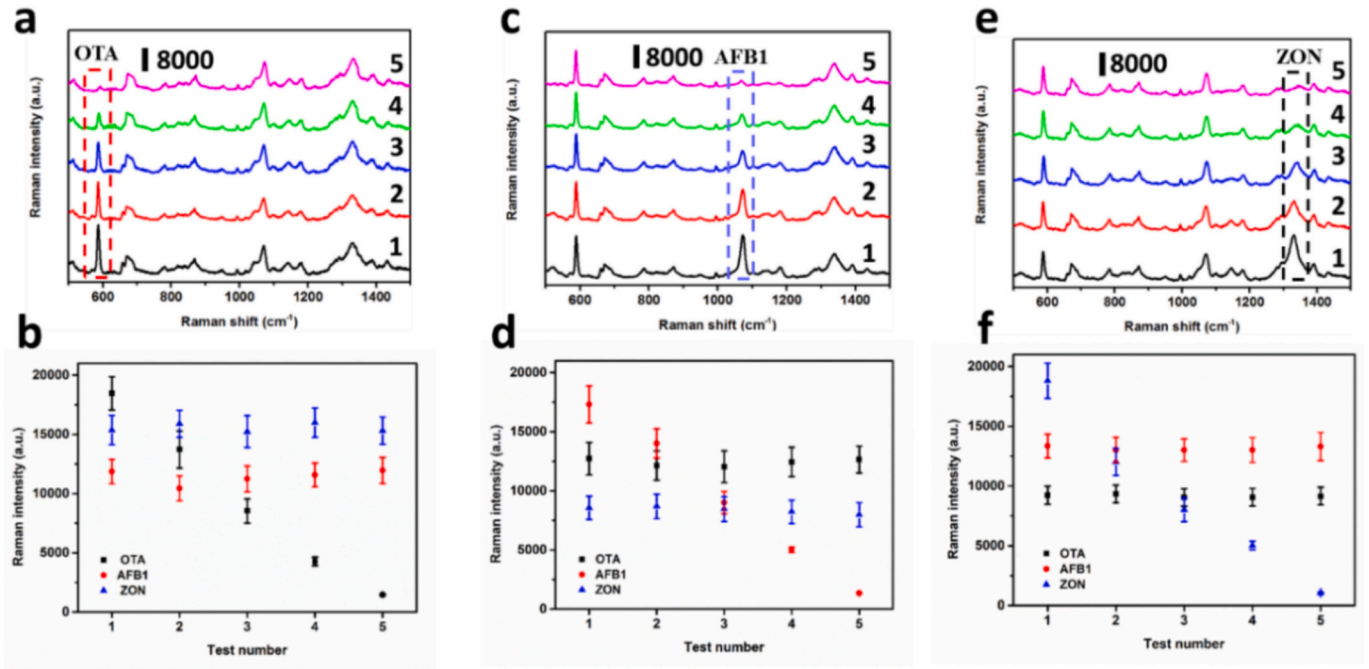

Fig. 8. Validation of the cross-reaction for multiplex mycotoxin detection. (a, c, and e) Raman spectra and (b, d, and f) Raman intensity at 593, 1076 and 1335 cm^{-1} with different concentrations of OTA, AFB1 and ZON. The concentrations annotated with '1, 2, 3, ……' were identical to the concentrations with the same number in Table S1(Supporting Information). Error bars were calculated from three repeats.

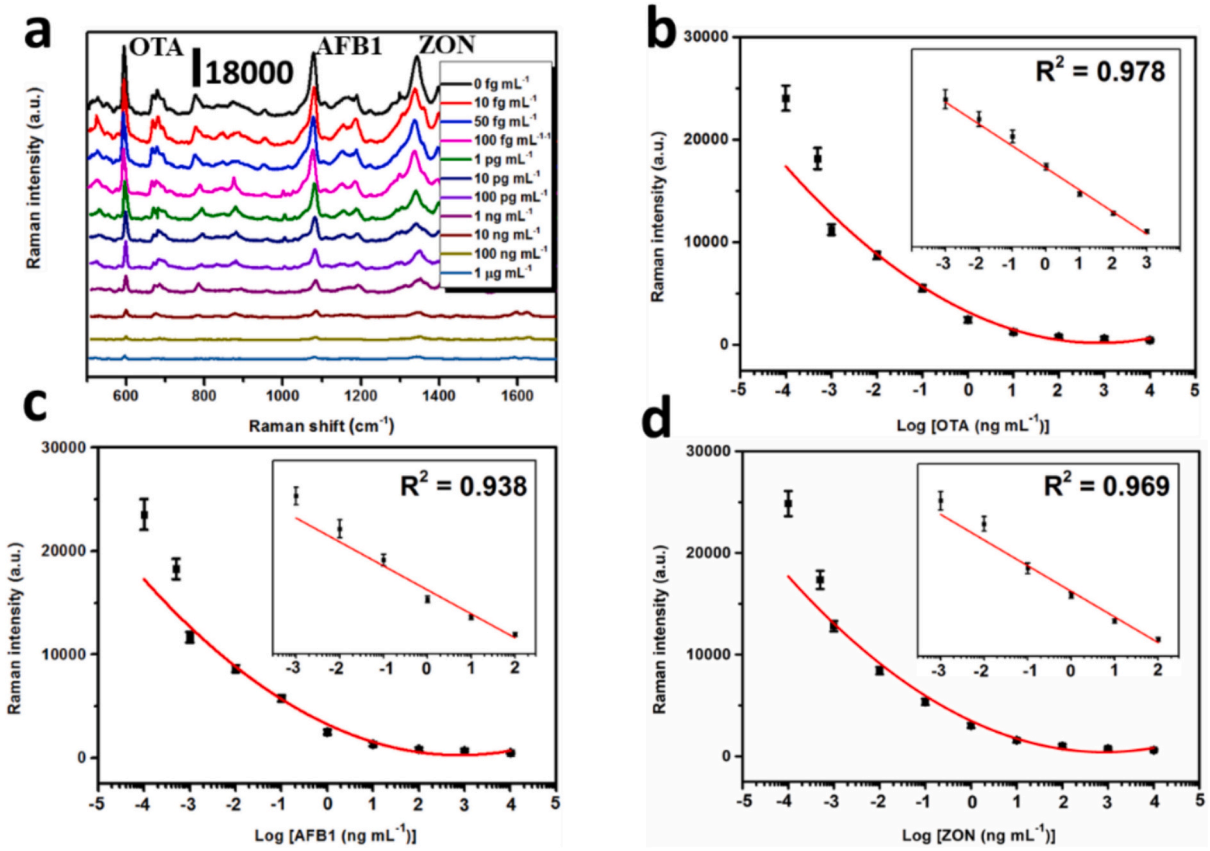

Fig. 9. SERS immunoassay for simultaneous detection of the multiplex mycotoxins OTA, AFB1 and ZON. (a) Mixed average SERS spectra for the simultaneous detection of different concentrations of OTA, AFB1 and ZON, with Raman intensities at 593, 1076 and 1335 cm^{-1}, respectively. (b, c, and d) Resulting calibration curves of OTA, AFB1 and ZON, respectively. The insets show the linear fit of the reference plots. Every measurement was performed in triplicate.

membrane-based SERS VFA, a spiked recovery experiment with a real food sample was carried out. The natural food preparation process are described in Materials and methods section. In brief, blank natural corn and wheat food samples were centrifuged for 15 min to prevent matrix interferences. The supernatant of the food sample was subsequently separated and spiked with various concentrations of AFB1, OTA and ZON. Quantitative analysis was subsequently performed with the developed SERS-based immunosensor. The results demonstrated that at spiking 0.2–10 ng mL^{-1} AFB1, 0.5–25 ng mL^{-1} OTA and 0.1–50 ng mL^{-1} ZON in cereals, the recoveries were 89.6 % to 100.2 %, 82.4 %–106.8 % and 81.0 %–107.1 %, respectively (Table S3, Supporting Information). Encouragingly, almost all the recovery rates of these samples were within the acceptable range of greater than 80 %. To further investigate the precision of the proposed method, ten naturally contaminated samples, including wheat, rice, corn, and peanuts were evaluated via the developed method and ELISA kits. In Figs. 10a, b and c the results of the assay revealed that the slopes of the regression equations and R-square values were close to 1, demonstrating that the developed method was consistent with ELISA. Therefore, we believe that the proposed SERS-based immunoassay biosensor has great potential for multiplex mycotoxin detection in cereal products. Although the PNC membrane-based SERS VFA biosensor seems to have good performance, problems related to fabricating the large-scale uniform ordered PNC membranes are still the limitations that need to be solved, and the design of SERS nanotags should be robust to ensure that the retrieved signal is accurate.

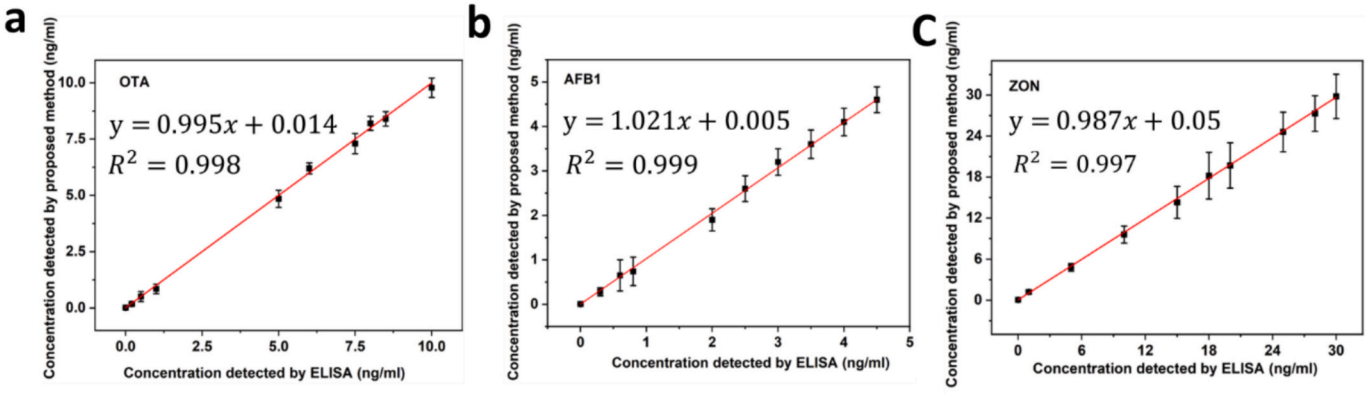

Fig. 10. The comparison between the proposed method and the ELISA method for (a) OTA, (b) AFB1 and (c) ZON detection in cereal samples.

4. Conclusions

In summary, a PNC membrane-based SERS VFA platform using Au^{NBA}@Ag, $Au^{4\text{-}MBA}$@Ag and Au^{DNTB}@Ag as labels for the detection of AFB1, OTA and ZON mycotoxins was described. The effects of the amount of $AgNO_3$ on the stability and SERS intensity of the SERS nanotag were investigated, and 0.1 mM was chosen as the optimum concentration in this study. For the fabrication of the ordered PNC membrane, the concentration of the NC solution and the stopband of PNC with different pore sizes were investigated. An NC concentration of 4 % (*w*/w) was chosen as the optimum condition, and the PNC membrane with a stopband of 632.4 nm was employed as the sensing substrate in the SERS VFA experiments. Furthermore, comparison of the immunoreaction performed on PNC with the NC membrane showed PNC with an ordered structure could greatly improve the detection sensitivity and SNR. This could be attributed to two reasons. First, the slow-photon effects of the PNC membrane promoted the coupling of excitation light with the SERS nanotags, which greatly improved the SERS intensity. The other reason was that the PNC membrane had a periodic nano-structure and a nanoconfinement effect that improved the binding kinetics of antigen-antibody in immune reactions, leading to more SERS nanotags being distributed on it. As a result, detection limits of 8.2, 3.7 and 47.6 fg mL^{-1} were obtained for the simultaneous detection of AFB1, OTA and ZON, respectively, which were lower than the EC-recommended tolerable cut-off values. Moreover, the specificity, recovery, and precision of this proposed method were stable and reliable, and it could be used for multiplex mycotoxin detection in agricultural products. In addition, this new technique could be easily employed for the detection of other toxins by controlling their corresponding target probes. Overall, the proposed method holds great promise for sensitive onsite food safety screening and is expected to have potential applications in government and market surveillance.

CRediT authorship contribution statement

Ruipeng Chen: Writing – original draft. **Jingfang Hu:** Data curation. **Hui Wang:** Investigation. **Cheng Li:** Conceptualization. **Haiqi Kang:** Formal analysis. **Yuxuan Chen:** Methodology, Conceptualization. **Liang Yang:** Resources. **Xiangfang Tang:** Visualization. **Benhai Xiong:** Visualization. **Xiangwei Zhao:** Funding acquisition.

Declaration of competing interest

The authors declare that they have no known competing financial interests or personal relationships that could have appeared to influence the work reported in this paper.

Data availability

The data that has been used is confidential.

Acknowledgements

This work was financially supported by the Technology Innovation 2030- Key Project of China (Grant No. 2021ZD0113801), the Central Public-interest Scientific Institution Basal Research Fund (no. 2022-YWF-ZYSQ-06), the Youth Teacher Research and Innovation Ability Enhancement Plan of Beijing University of Agricultural (QJKC-2022053) and the Fundamental Research Project of Shenzhen Science & Technology Innovation Committee (JCYJ20230807114610021).

Appendix A. Supplementary data

Supplementary data to this article can be found online at https://doi.org/10.1016/j.fochx.2024.102152.

References

Aichinger, G., Pantazi, F., & Marko, D. (2020). Combinatory estrogenic effects of bisphenol a in mixtures with alternariol and zearalenone in human endometrial cell. *Toxicology Letters, 319*, 242–249.

Berger, A., Restaino, S., & White, I. (2017). Vertical-flow paper SERS system for therapeutic drug monitoring of flucytosine in serum. *Analytica Chimica Acta, 949*, 59–66.

Chen, J., Freymann, G., Choi, S., Kitaev, V., & Ozin, G. (2008). Slow photons in the fast lane in chemistry. *Journal of Materials Chemistry, 18*, 369–373.

Chen, R., Du, X., Cui, Y., Zhang, X., Ge, Q., Dong, J., & Zhao, X. (2020). Vertical flow assay for inflammatory biomarkers based on nanofluidic channel array and SERS nanotags. *Small, 16*, Article 2070180.

Chen, R., Liu, B., Ni, H., Chang, N., Luan, C., Ge, Q., … Zhao, X. (2019). Vertical flow assays based on core-shell SERS nanotags for multiplex prostate cancer biomarker detection. *Analyst, 144*, 4051–4059.

Chi, J., Gao, B., Sun, M., Zhang, F., Su, E., Liu, H., & Gu, Z.. (2017). Patterned photonic nitrocellulose for pseudopaper ELISA. *Analytical Chemistry, 89*, 7727–7733.

Clarke, O., Goodall, B., Hui, H., Vats, N., & Brosseau, C. (2017). Development of a SERS-based rapid vertical flow assay for point of-care diagnostics. *Analytical Chemistry, 89*, 1405–1410.

Curti, M., Mendive, C., Grela, M., & Bahnemann, D. (2017). Stopband tuning of TiO_2 inverse opals for slow photon absorption. *Research Bulletin, 91*, 155–156.

EC. (2006). Setting maximum levels for certain contaminants in foodstuffs. In *Commission regulation (EC) no 1881/2006; European Commission regulation*. Brussels.

Fan, S., Villeneuve, P., Joannopoulos, J., & Schubert, E. (1997). High extraction efficiency of spontaneous emission from slabs of photonic crystals. *Physical Review Letters, 78*, 3294–3297.

Frens, G. (1973). Controlled nucleation for the regulation of the particle size in monodisperse gold suspensions. *Nature Physical Sciences, 241*, 20–22.

Gao, B., Liu, H., & Gu, Z. (2016). Patterned photonic nitrocellulose for pseudo-paper microfluidics. *Analytical Chemistry, 88*, 5424–5429.

Gellner, M., Kömpe, K., & Schlücker, S. (2009). Multiplexing with SERS labels using mixed SAMs of Raman reporter molecules. *Analytical and Bioanalytical Chemistry, 394*, 1839–1844.

Guo, Z., Wang, M., Wu, J., Tao, F., Chen, Q., Wang, Q., Ouyang, Q., Shi, J., & & Zou, X. (2019). Quantitative assessment of zearalenone in maize using multivariate algorithms coupled to Raman spectroscopy. *Food Chemistry, 286*, 282–288.

Huang, Z., Meng, G., Huang, Q., Yang, Y., Zhu, C., & Tang, C. (2010). Improved SERS performance from au nanopillar arrays by abridging the pillar tip spacing by ag sputtering. *Advanced Materials, 22*, 4136–4139.

Jalalian, S., Karimabadi, N., Ramezani, M., Abnous, K., & Taghdisi, S. (2018). Electrochemical and optical aptamer-based sensors for detection of tetracyclines. *Trends in Food Science and Technology, 73*, 45–57.

Kearns, H., Goodacre, R., Jamieson, L., & Faulds, K. (2017). SERS detection of multiple antimicrobial-resistant pathogens using nanosensors. *Analytical Chemistry, 89*, 12666–12673.

Krug, J., Wang, G., Emory, S., & Nie, S. (1999). Efficient Raman enhancement and intermittent light emission observed in single gold nanocrystals. *Journal of the American Chemical Society, 121*, 9208–9214.

Kuo, C., Lu, S., Chen, S., Bernards, M., & Jiang, S. (2007). Stop band shift based chemical sensing with three-dimensional opal and inverse opal structures. *Sensors and Actuators B: Chemical, 124*, 452–458.

Lai, W., Wei, Q., Xu, M., Zhuang, J., & Tang, D. (2017). Enzyme-controlled dissolution of MnO_2 nanoflakes with enzyme cascade amplification for colorimetric immunoassay. *Biosensors & Bioelectronics, 89*, 645–651.

Lin, Y., Chen, C., & Lin, M. (2018). Enzyme-free amperometric method for rapid determination of histamine by using surface oxide regeneration behavior of copper electode. *Sensors and Actuators B: Chemical, 255*, 2838–2843.

Liu, B., Ni, H., Zhang, D., Wang, D., Fu, D., Chen, H., Gu, Z., & & Zhao, X. (2017). Ultrasensitive detection of protein with wide linear dynamic range based on core-shell SERS nanotag and photonic crystal beads. *ACS Sensors, 2*, 1035–1043.

Liu, Y., Li, W., Ding, Z., Li, Q., Wang, X., Liu, J., Zhou, S., Shao, R., ling, Q., Zheng, T., & Li, J. (2019). Three-dimensional ordered macroporous magnetic photonic crystal microspheres for enrichment and detection of mycotoxins (II): The application in liquid chromatography with fluorescence detector for mycotoxins. Journal of Chromatography. A, 1604, 1–8.

Mažeikienė, R., Niaura, G., Eicher-Lorka, O., & Malinauskas, A. (2019). Raman spectroelectochemical study of electrode reactions of hydroquinone at electrodes modified with Nile blue and other azine type redox mediators. *Journal of Solid State Electrochemistry, 23*, 2307–2316.

Mu, Z., Zhao, X., Huang, Y., & Lv, M. (2015). Photonic crystal hydrogel enhanced plasmonic staining for multiplexed protein analysis. *Small, 11*, 6036–6043.

Nath, P., & Ray, A. (2023). Nanotechnology-based strategies for advancing point-of-care lateral flow immunoassays. *Current Opinion in Biomedical Engineering, 28*, 100504–100513.

Radmark, M., Elgcrona, G., & Karlsson, H. (2020). Novel narrow linewidth 785 nm diode laser with enhanced spectral purity facilitates low-frequency Raman spectroscopy. *SPIE BIOS, 11252*.

Regiart, M., Vicario, O., Villarroel-Rocha, J., Sapag, K., Messina, G., Raba, J., & Bertolino, F. (2018). Mesoporous immunosensor applied to zearalenone determination in *Amaranthus cruentus* seeds. *Microchemical Journal, 141*, 388–394.

Santis, B., Debegnach, F., Gregori, E., Russo, S., Marchegiani, F., Moracci, G., & Brera, C. (2017). Development of a LC-MS/MS method for the multi-mycotoxin determination in composite cereal-based samples. *Toxins, 9*, 169–181.

Song, S., Kim, D., Kim, J., You, J., & Kim, H. (2021). Flexible nanocellulose-based SERS substrates for fast analysis of hazardous materials by spiral scanning. *Journal of Hazardous Materials, 414*, Article 125160.
Sumioka, K., Kayashima, H., & Tsutsui, T. (2002). Tuning the optical properties of inverse opal photonic crystals by deformation. *Advanced Materials, 14*, 1284–1286.
Sun, L., Yang, M., Huang, J., Yu, D., Hong, W., & Chen, X. (2016). Freestanding graphitic carbon nitride photonic crystals for enhanced photocatalysis. *Advanced Functional Materials, 26*, 4943–4950.
Tuschel, D. (2016). Selecting an excitation wavelength for Raman spectroscopy. *Spectroscopy, 31*, 14–23.
Yu, J., Lei, J., Wang, L., Zhang, J., & Liu, Y. (2018). TiO_2 inverse opal photonic crystals: Synthesis, modification, and applications. *Journal of Alloys and Compounds, 769*, 740–757.
Zelsmann, M., Picard, E., Charvolin, T., & Hadji, E. (2003). Seventy-fold enhancement of light extraction form a defectless photonic crystal made on silicon-on-insulator. *Applied Physics Letters, 83*, 2542–2544.
Zhang, D., Huang, L., Liu, B., Ge, Q., Dong, J., & Zhao, X. (2019). Vertical flow microarray chip based on SERS nanotags for rapid and ultrasensitive quantification of α-fetoprotein and carcinoembryonic antigen. *Microchimica Acta, 186*, 699.
Zhao, Y., Zhao, X., Hu, J., Xu, M., Zhao, W., Sun, L., … Gu, Z. (2009). Encoded porous beads for label-free multiplex detection of tumor markers. *Advanced Materials, 21*, 569–572.
Zhou, L., Liu, Y., Wang, F., Jia, Z., Zhou, J., Jiang, T., … Wang, X. (2018). Classification analyses for prostate cancer, benign prostate hyperplasia and healthy subjects by SERS based immunoassay of multiple tumour markers. *Talanta, 188*, 238–244.
Zinedine, A., Soriano, J., Molto, J., & Manes, J. (2007). Review on the toxicity, occurrence, metabolism, detoxification, regulations, and intake of zearalenone: An oestrogenic mycotoxin. *Food and Chemical Toxicology, 45*(1), 1–18.